PNL-SA-7771

CONF-790808--22

MASTER

AIR VELOCITY PROFILES NEAR SLEEVE BLOCKAGES IN AN UNHEATED 7 X 7 ROD BUNDLE

J. M. Creer
J. M. Bates

April 1979

Submitted for presentation to the
American Society of Mechanical Engineers
Symposium on Fluid Flow and
Heat Transfer over Rod or Tube Bundles

Aug. 5-9, '79

Work Supported by
the U.S. Nuclear Regulatory Commission
under a Related Services Agreement with
the U.S. Department of Energy
under Contract EY-76-C-06-1830

Pacific Northwest Laboratory
Richland, Washington 99352

DISCLAIMER

AIR VELOCITY PROFILES NEAR SLEEVE BLOCKAGES IN AN UNHEATED 7 x 7 ROD BUNDLE

J. M. CREER
J. M. BATES

Pacific Northwest Laboratory
Richland, Washington

ABSTRACT

Local air velocity measurements were obtained with a laser Doppler anemometer near flow blockages in an unheated 7x7 rod bundle. Sleeve blockages were positioned on the center nine rods to create an area reduction of 90% in the center four subchannels of the bundle. Experimental results indicated that severe flow disturbances occurred downstream from the blockage cluster but showed only minor flow disturbances upstream from the blockage. Flow reversals were detected downstream from the blockage and persisted for approximately five subchannel hydraulic diameters. The air velocity profiles were in excellent agreement with water velocity data previously obtained at essentially the same Reynolds number. Subchannel average velocity predictions obtained with the COBRA computer program were in good agreement with subchannel average velocities estimated using the measured local velocity data.

NOMENCLATURE

English

- $\widehat{BLC}$ - blockage axial centerline
- DP - designates data plane
- Eu - Euler number, $U_B(\rho/2g\ \Delta P)^{1/2}$
- f - friction factor
- f_i - frequency of incident laser beam
- f_D - Doppler frequency
- f_{s1}, f_{s2} - frequency shift
- ft - turbulent momentum factor
- K_{ij} - crossflow resistance
- K_{s1} - subchannel spacer loss coefficient
- K_{s2} - subchannel blockage loss coefficient
- ΔP - pressure loss
- Re_B - Bundle Reynolds number
- s/ℓ - transverse momentum
- t - time
- T - temperature
- $\overline{u}$ - local mean axial velocity
- $U_B, \overline{UB}$ - bundle average velocity
- $\overline{U}$ - subchannel average velocity
- x - x coordinate
- y - y coordinate
- z - z coordinate
- Δz - calculational increment

Greek

- β - turbulent mixing
- λ - wavelength
- ρ - density
- θ - angle between incident laser beams.

INTRODUCTION

In the event of a loss-of-coolant accident (LOCA) in a pressurized water reactor (PWR), fuel rod overheating may occur. As clad temperatures increase during a LOCA, internal fuel rod pressures may cause clad "swelling" or "ballooning," which could lead to coolant blockages. It is important that flow and heat transfer phenomena near such blockages are well understood to permit detailed safety analyses to be performed for postulated LOCAs. Consequently, as a first step in gaining such an understanding, a program was initiated to study the effects of blockages on flow distributions in rod bundles. The program objectives were: 1) to evaluate, develop, and apply laser Doppler anemometry (LDA) methods for measuring flow and turbulence in the vicinity of blockages and 2) to improve the data base for evaluating subchannel (core) codes such as COBRA (1,2). The intent of the program was to perform a logical sequence of flow blockage experiments using water, air, air-water, and steam-water in model nuclear fuel rod bundles. Such information was limited for relatively large rod bundles in any of the above-mentioned flowing media. In addition to providing basic subchannel velocity and turbulence data that could be related to blockages under flowing steam conditions in reactor accident environments, it was anticipated that the LDA experiments using single-phase water and air could aid in developing state-of-the-art two-phase flow instrumentation. Such instrumentation could subsequently be used in studies using air-water and, finally, using steam-water flow typical of that expected during a LOCA.

The current study, using air as the flowing medium, was a follow-on to the study reported in References (3) and (4) where water was used as the working fluid and two blockage severities plus two blockage locations were investigated. The abbreviated study reported herein incorporated the same experimental method used in the water test, but only one blockage severity (90%) at one axial location within the bundle was investigated. The air conditions, $Re_B = 1 \times 10^4$, approximated those of steam at a point in time during a postulated LOCA at which all of the flooding water (1.27 cm/sec, 0.5 in./sec) would be converted to high quality steam.

This paper presents air velocity profiles obtained near a partial flow blockage. Comparisons of the air velocity profiles with water velocity profiles obtained in a previous experiment and

comparisons of the experimental velocity data with predictions of the COBRA code are provided.

EQUIPMENT

The basic equipment used to perform the flow blockage experiment consisted of an air loop, a test assembly made up of a flow housing and an unheated 7x7 rod bundle, a laser Doppler anemometer, and signal processing instrumentation. The following sections briefly discuss the equipment used in the study.

Air Loop

The flow blockage experiment was performed in the air loop shown schematically in Fig. 1. A blower rated at 366 ℓ/sec (775 cfm) at 124 KPA (18 psig) was used to produce the desired air flow rate through the test assembly. An after-cooler was provided to attain an air operating temperature of 27°C (80°F). Three flow control devices--a damper, a control valve, and a bypass valve--were used to obtain the test flow rate as measured with an orifice meter/pressure transducer combination. Temperatures and absolute pressures were measured just upstream of the orifice meter and at the test assembly inlet. After the air passed through the test assembly, it was exhausted to the atmosphere through a large 0.3-m (12-in.) duct.

Ammonia chloride light-scattering particles were injected into the piping system just upstream of the test section. Air was used to agitate hydrochloric acid and ammonia hydroxide to permit mixing their vapors in a tube to form stable ammonia chloride particles. Control valves on the supply lines to the mixing tube were provided to permit proper mixture ratios and seeding flow rates.

Test Assembly

The test assembly used in the air study is shown in Fig. 2. Air entered the bottom of the flow housing, flowed vertically upward through the bundle, emerged at the top of the flow housing, and entered the exhaust duct. A 0.2-m (8-in.) long flow

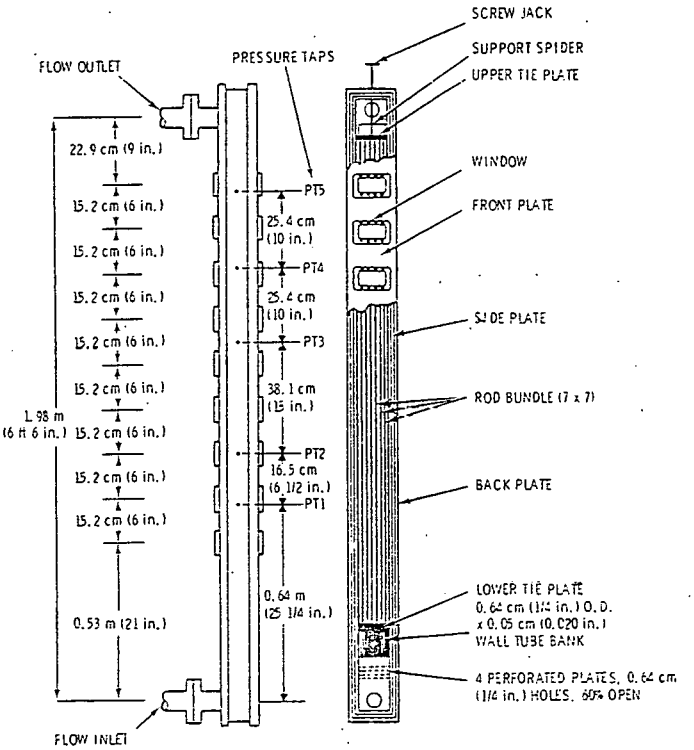

Fig. 2 Test assembly arrangement

conditioning section was placed at the test assembly inlet. The flow conditioner consisted of four eccentric perforated plates in a triangular array, followed by a bank of tubes 8.25 cm (3.25 in.) long. The plates distributed the flow uniformly across the test assembly cross section; the tubes served as flow straighteners to limit the scale of turbulence.

A cross-sectional view of the assembly at the blockage axial centerline is presented in Fig. 3. The flow housing body consisted of front and back plates containing nine windows and solid stainless

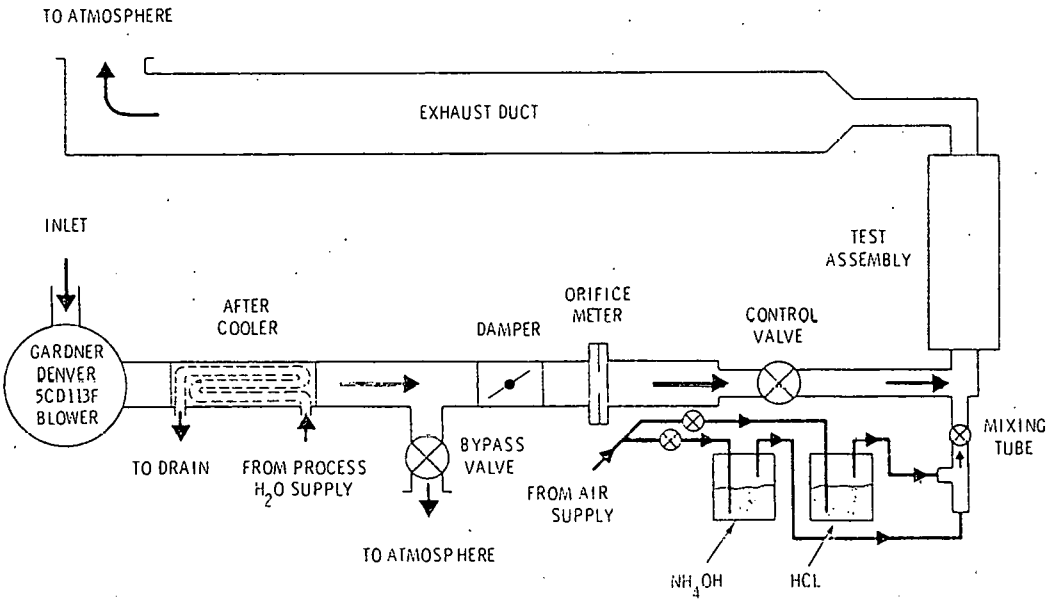

Fig. 1 Air loop

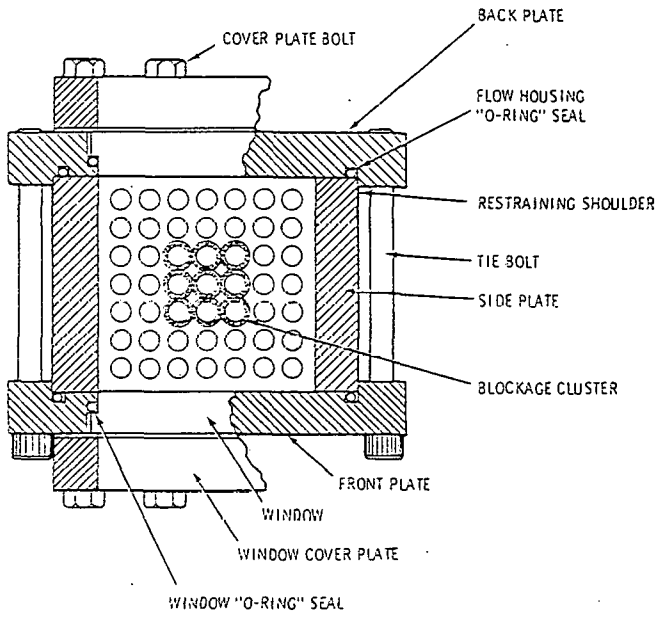

Fig. 3. Test assembly cross section at the blockage axial centerline

steel side plates containing pressure taps. The windows were 5.1 cm (2 in.) high by 10.2 cm (4 in.) wide, and were located on 15.2-cm (6-in.) axial intervals. The optically flat and parallel windows were fabricated from borosilicate crown glass, sealed with O-rings, and held in place by thick cover plates.

The model fuel bundle was an unheated square 7x7 rod array. Model unheated rods were fabricated from 0.318-cm (1/8-in.) Sch 10S stainless steel pipe [OD = 1 cm (0.392 in.)] 1.45 m (57 in.) long. Lower and upper brass tie plates positioned the 49 rods to form the bundle. Flow channels in the tie plates were sized to assure uniform velocity distributions over the cross section of the bundle. A rod pitch of 1.37 cm (0.539 in.) was maintained with three simple "egg crate" spacers fabricated from brass.

Brass sleeves were placed on the center nine rods to model a blockage cluster as shown in Fig. 4. The blockages were 7.623 cm (3 in.) long with 2.54-cm (1-in.) tapers at each end. A flow area reduction of 90% was attained in the center four subchannels of the bundle. The 90% severity corresponded to an area reduction of 45% in the subchannels adjacent to the sides of the cluster and 22% in the subchannels next to the corners of the blockage. The shape, location, and extent of area reduction of the blockage cluster used in this experiment were not necessarily intended to define those that would actually exist during a LOCA. The shape of the blockage sleeves was formulated after considering Hardy's experimental results of high temperature expansion and rupture behavior of Zircaloy tubing (5). Area reductions of 70% and 90% were chosen to create gross flow disturbances in the rod bundle. Gross flow disturbances were required to adequately test the capability of the COBRA computer program for predicting such maldistributed flow profiles. Determination of more realistic blockage locations, shapes and severities must await results of experiments designed to obtain such information.

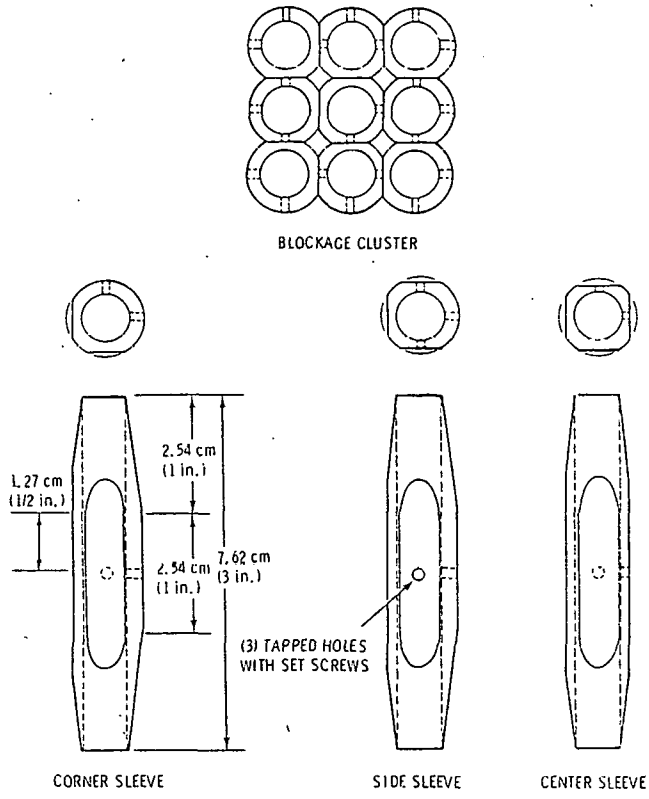

Fig. 4 Flow blockage sleeves

A movable support was provided at the top of the bundle to position the rod bundle in the flow housing. A vertical travel of 17.8 cm (7 in.) was possible and, because the windows were on 15.21-cm (6-in.) centerlines, data at any axial location within the bundle could be obtained.

Laser Doppler Anemometer

Turbulent flow measurements were performed with a laser Doppler anemometer (LDA), a highly advanced system used for obtaining measurements of local mean velocity and intensity of turbulence. The most notable advantage of an LDA system is that the noncontact probing does not disturb the flow. An important feature of all LDA systems is that the output signal is a calibration-free frequency linearly related to flow velocity. Single known components of flow velocity can be measured independently of other velocity components; furthermore, velocity measurements in reversing flows are possible.

The LDA system used in this experiment is shown schematically in Fig. 5; the theoretical aspects of the method are discussed in detail by Brayton and Geothert (6). The differential Doppler mode with frequency shifting was used throughout the experiment. The system is easily aligned and operates effectively where the intensity of scattered light is low. Frequency shifting removed the directional ambiguity, allowing measurements in regions of reverse flow. Ammonia chloride particles injected in the loop air were used as light-scattering particles in this experiment.

The measuring, or intersection, volume was located in the flow channel with a hydraulic lift/traversing table capable of positioning the laser and optics as an integral unit. The motor

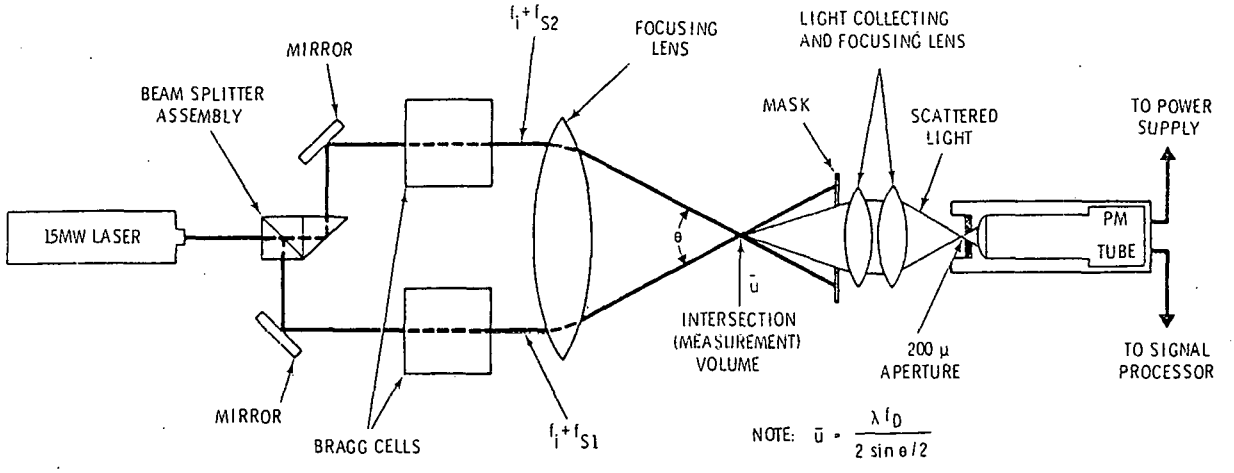

Fig. 5 Differential doppler laser Doppler anemometry system

speed control and position control inherent in the table made it possible to locate the beam intersection volume to within 0.00254 cm (0.001 in.) in both the x and y coordinates in a horizontal plane. The hydraulic lifting capability of the table permitted the laser and optics to be positioned at desired axial locations.

Signal Processing Instrumentation

The signal processing instrumentation used to condition, interpret, and obtain the axial velocity data from the Doppler signal basically consisted of a spectrum analyzer with a tracking generator, a frequency tracker, and an oscilloscope.

The spectrum analyzer/tracking generator combination was used as the primary data acquisition device because the frequency tracker did not operate satisfactorily in regions of highly turbulent air flow. The spectrum analyzer received a signal from the photomultiplier tube and a frequency spectrum (signal amplitude versus frequency) was displayed on the CRT. The tracking generator, a special signal source whose rf output frequency tracks (follows) other signals in the frequency domain, was then used to accurately read the Doppler frequency corresponding to the peak amplitude as measured by the spectrum analyzer.

The frequency tracker was used as a back-up unit to the spectrum analyzer because it would not "hold track" in regions of highly turbulent air flow. When in use, the frequency tracker improved the signal-to-noise ratio of the Doppler signal and converted the Doppler frequency into an analog voltage that was linearly related to local mean axial flow velocity. The tracker had frequency tracking capabilities in that, once it was "locked-on" to the Doppler frequency, it followed frequency fluctuations about the mean within each available frequency range. An LED readout was supplied on the tracker; however, a digital voltmeter was used to measure tracker analog voltage output to obtain more accurate determinations of Doppler frequencies.

EXPERIMENTAL PROCEDURE

Loop flow and temperature were set at desired values. The LDA optical system was adjusted to produce an optimal Doppler signal as observed on an oscilloscope. Data acquisition was started approximately 0.254 cm (0.100 in.) from a window and continued incrementally, usually every 0.254 cm (0.100 in.), along selected traverses across the rod bundle as shown in Fig. 6. Only data obtained along the traverse at y = 4.48 cm (1.763 in.) are presented in this paper. Data obtained along each traverse are presented by Creer et al (7).

At each data location the spectrum analyzer and frequency tracker were checked to assure proper adjustment. The spectrum analyzer frequency, tracker voltage, x and y locations, and other pertinent loop information were then recorded. The lift/traversing table was then used to reposition the measuring volume to other axial locations and the above procedure was repeated.

DATA ACCURACY

An error analysis using the error and uncertainty methods of Schenk (8) was performed to estimate data accuracy. The method and analysis are presented and described in detail in (7). Local mean axial velocity measurements ($\bar{u}$) were estimated to have uncertainties of $\leq \pm 6\%$. Data point locations adjacent to the windows were located within ±1.27 mm (±0.05 in.) of the window. Data traverses adjacent to a rod row were located relative to the rods within ±0.25 mm (0.01 in.). Each measurement location was positioned within

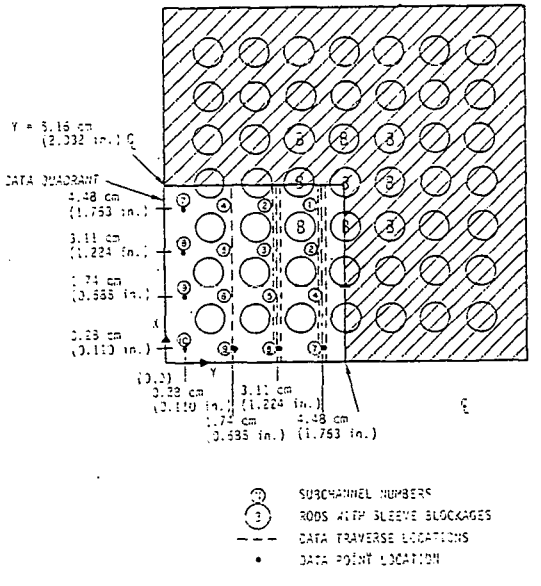

Fig. 6 Data traverse locations

±0.025 mm (0.001 in.) of its neighbors in the x and y directions. Axial data planes were estimated to be located within ±1.27 mm (0.05 in.) of the blockage axial centerline.

EXPERIMENTAL RESULTS AND DISCUSSION

Velocity Reduction and Recovery

Velocity profiles obtained at specific axial distances (data planes) upstream of the 90% blockage cluster are presented in Fig. 7. Each of the plots in Fig. 7 presents local mean axial velocities normalized relative to bundle average velocity as functions of distance from the wall (x = 0 corresponds to the wall). Each data traverse was obtained at y = 4.48 cm (1.763 in.) as indicated in the cross-sectional view of the bundle. Distances accompanying the data plane designations indicate upstream locations (negative sign) relative to the blockage axial centerline.

At a location 21.6 cm (8.5 in.) upstream of the blockage centerline, ≈1.9 cm (0.75 in.) downstream of Spacer 1, the velocity profile shows the effects of the spacer by its "ragged" appearance and a peak-to-average velocity ratio of ∿1.1. At an axial location 12.2 cm (4.8 in.) upstream of the blockage cluster, the velocity profile shows consistent peaks at subchannel centers and valleys at rod gaps. Axial velocity peak-to-average ratios of ∿1.2 were measured which are in good agreement with those known to exist for well developed turbulent pipe flow and existing rod bundle data (3,4,9,10,11). The velocity profile indicates that the flow conditioning section at the test assembly entrance distributed the flow uniformly across the bundle cross section.

In the tapered region of the blockage, 3.3 and 4.3 cm (1.3 and 1.7 in.) upstream of the centerline, the influence of the blockage cluster was present, as indicated by the relatively low velocities in the inner subchannels and the higher velocities in the outer subchannels. Velocity ratios in the innermost subchannel, Subchannel 1 (SC 1), decreased from ∿1.2 to ∿0.15. Low velocities are realizable because SC 1 had an area reduction of 90% and flow was forced around the blockage cluster. Peak-to-average velocity ratios in the outer subchannels increased from ∿1.2 to ∿1.3, which also indicates that flow was being diverted around the blockage.

Velocity profiles obtained immediately downstream of the blockage cluster are presented in Fig. 8. Note that downstream locations are designated by the plus sign preceding the data plane distance values. Velocity distributions obtained 3.30, 3.81, and 6.35 cm (1.3, 1.5, and 2.5 in.) downstream of the blockage centerline indicate that

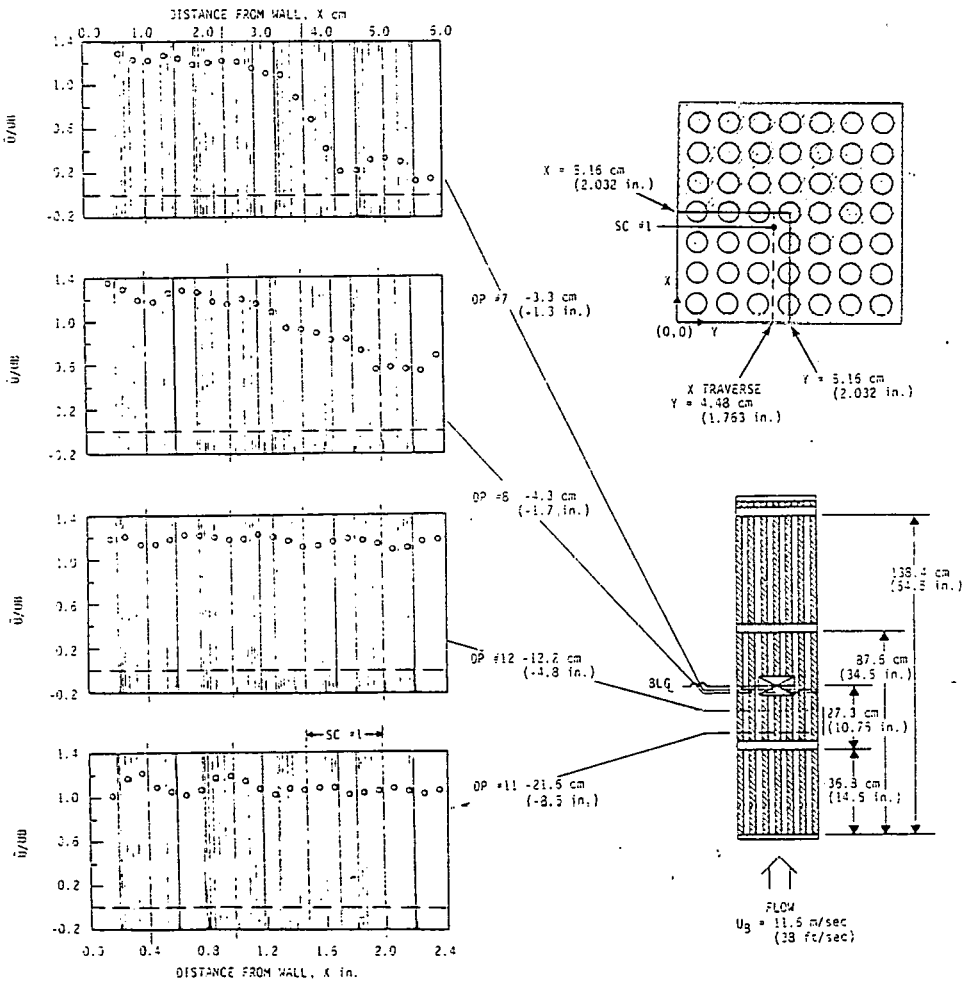

Fig. 7 Velocity profiles upstream of a 90% blockage located midway between two spacers, U_B = 11.6 m/sec (38 ft/sec) ($Re_B = 1x10^4$)

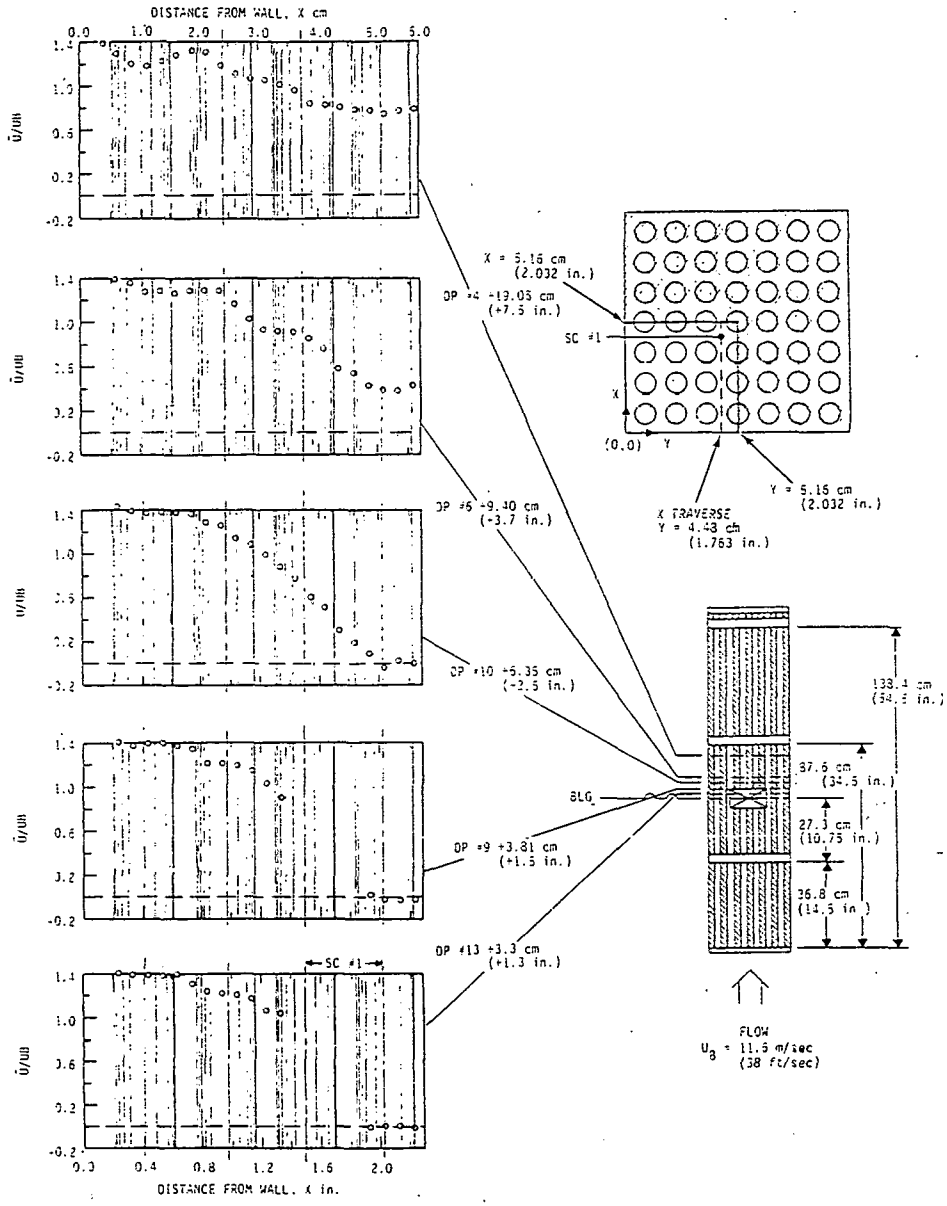

Fig. 8 Velocity profiles immediately downstream of the 90% blockage located midway between two spacers, U_B = 11.6 m/sec (38 ft/sec) ($Re_B = 1x10^4$)

zero and negative flows were measured. The flow reversal defines a recirculation zone confined to SC 1 in the lateral direction. The low inner subchannel velocities were accompanied by relatively high outer subchannel velocities, as indicated by the high peak-to-average velocity ratios of ∿1.4. Axially, the recirculation zone persisted for at least 6.35 cm (2.5 in., ∿5 subchannel hydraulic diameters) downstream of the blockage centerline. Flow reversals were not detected 8.64 cm (3.4 in., ∿7 diameters) downstream of the blockage cluster, and flow recovery was significant 19.05 cm (7.5 in.) downstream of the blockage centerline.

The data points not included in the velocity profiles at Data Planes 9 and 13 are missing because the flow was very turbulent, making it impossible to obtain Doppler signals. The frequency spectrum actually disappeared from the spectrum analyzer CRT screen and the frequency tracker could not follow the Doppler frequency. Note that the signal was lost at the entrance to SC 1, but was regained near the rod gap corresponding to the bundle centerline.

Velocity Profiles at One Axial Location

Velocity profiles measured along all data traverses obtained at a single cross section, Data Plane 10, are presented in Fig. 9 to indicate the local characteristic of the recirculation zone in the lateral direction. The lower plot contains velocity profiles obtained at y = 4.48 and 3.11 cm (1.763 and 1.224 in.). Velocity magnitudes are relatively high in the outer subchannels along each traverse. Velocity profiles in the inner subchannels at y = 4.48 cm (1.763 in.) indicate that zero and negative velocities existed, i.e., a recirculation zone was detected. Velocities obtained in inner subchannels at y = 3.11 cm (1.224 in.) were not negative, indicating that the recirculation zone was restricted to the 90% blocked subchannel (SC 1) in the lateral direction.

Velocities presented in the upper plot of Fig. 9 were obtained in the outer subchannels of the bundle at y = 1.74 and 2.79 cm (0.685 and 0.110 in.). The outer subchannel velocities are relatively high, because flow was diverted around the blockage cluster.

Comparison of Air and Water Velocity Data

Velocity Reduction and Recovery. In Fig. 10, air velocity data obtained in this experimental study are compared to water velocity data reported in References (3) and (4). The Reynolds and Euler numbers of the flowing air ($Re_B \approx 1.0 \times 10^4$, $Eu \approx 0.42$) were approximately equal to those of the water ($Re_B \approx 1.4 \times 10^4$, $Eu \approx 0.44$). In the upstream tapered region of the blockage cluster -3.3 cm (-1.3 in.), the air and water velocity profiles obtained along an x traverse at y = 4.48 cm (1.763 in.) essentially coincide. In the downstream tapered region, +3.3 cm (+1.3 in.), the two velocity profiles are in good agreement; however, the water profile contains some scattered velocity data points. Farther downstream from the blockage axial centerline, the air and water profiles compare well.

It can be seen that, in outer subchannels, x < 2 cm (0.8 in.), normalized air velocities were consistently higher than normalized water

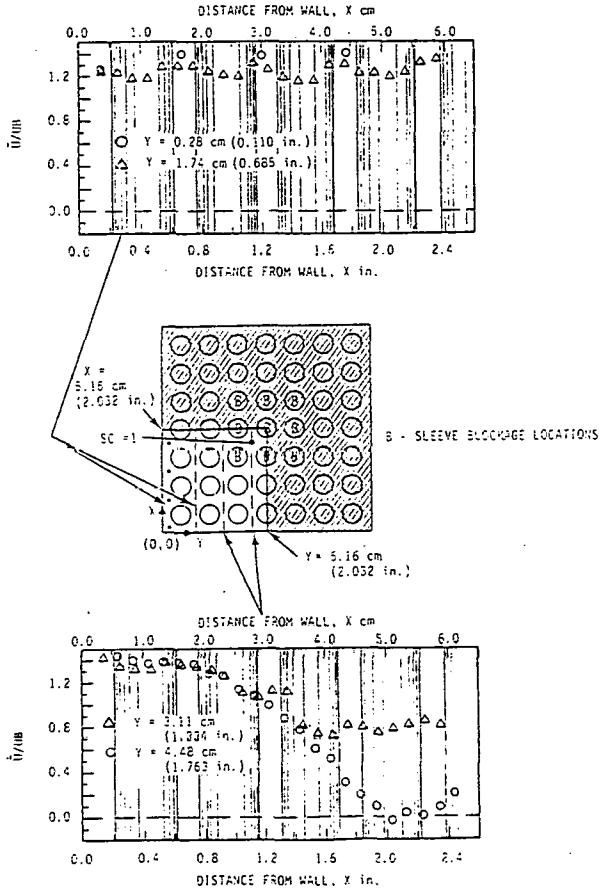

Fig. 9 Velocity profiles at Data Plane 10 (6.35 cm, +2.5 in.) with a 90% blockage, U_B = 11.6 m/sec (38 ft/sec) ($Re_B = 1 \times 10^4$)

velocities. No final conclusion has been formulated as to the cause of the higher air velocities. A possible explanation for this difference could be that ammonia chloride particles collected on the windows during the air experiment and, due to extraneous scattered light, may have affected measurements in the wall subchannels. The difference is of minor significance and does not affect the major results of the study.

Perhaps a better mental picture of what the velocity reduction and recovery profiles along the length of the bundle actually were can be conveyed by examining Fig. 11. Normalized Subchannel 1 center velocities are presented along the length of the bundle for both air data and existing water data (3,4). For the most part, the axial velocity profiles are in excellent agreement. The upstream and downstream minimum velocity magnitudes and locations coincide with one another.

Velocity Profiles at a Selected Axial Location. Figure 12 presents velocity profiles obtained in air and those obtained in water (3,4) at an axial distance 6.35 cm (2.5 in.) downstream from the blockage axial centerline. As shown, the velocity profiles are in good agreement with the exception of those obtained at y = 3.1 cm (1.224 in.) where same data scatter was encountered. The traverses at y = 3.1 cm (1.224 in.) were midway between a rod row in which inner rods contained blockage sleeves and a row without blockages. The nonsymmetrical disturbances created in the inner subchannels are thought to be the cause of the data scatter.

COMPARISONS WITH COBRA PREDICTIONS

Comparisons of the measured velocity data with predictions obtained using the COBRA code are presented in this section. The comparisons are of major importance in the continuing development of the COBRA code for subchannel (core) analyses at postulated nuclear reactor accident conditions. Similar measured and predicted velocity comparisons were performed using water in a previous investigation (3,4) and it was confirmed that COBRA could predict water velocities satisfactorily with a blockage located midway between two spacers. Such a confirmation is required for low density air flow to add to the data base required for future analyses of two-phase steam-water flows expected to exist during actual LOCAs.

COBRA Version and Input Model

The local air velocity data could not be predicted with COBRA-IIIC (1) using standard steady-state techniques because instabilities in the numerical solution were encountered. Therefore, predictions of the velocity data were performed with a modified version of COBRA-IIIC using a "two-step" approach as follows:

1. Steady-state predictions with a 70% blockage were performed.

2. A transient solution, which extended the 70% blockage solution to a 90% blockage solution, was then performed. During each transient time increment, a slightly greater blockage severity was introduced into the input geometry. After a 90%

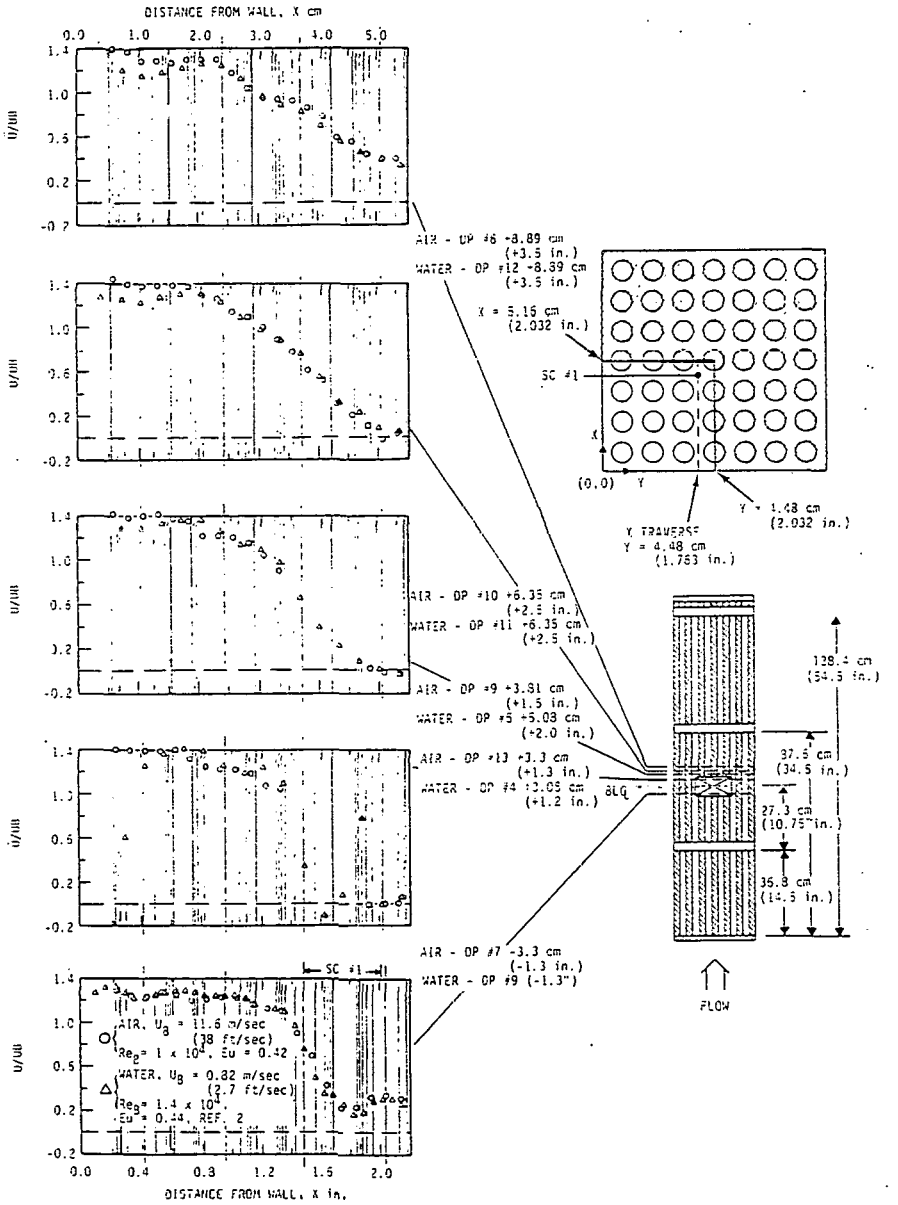

Fig. 10 Comparisons of air velocity data with water velocity data near a 90% blockage located midway between two spacers

severity had been obtained, sufficient time steps were completed to assure convergence to the correct solution. It is important to note that the solution was transient with respect to blockage severity only, and that all other input parameters remained constant with time.

The input parameters used to predict the axial velocity data are summarized in Table 1. As indicated, the values of the parameters are typical of those commonly used in nonheated bundle predictions. The blockage loss coefficients were those determined in (3) and (4). They were varied from subchannel to subchannel and ranged from 0 to 0.5, depending on subchannel location relative to the blockage cluster. The spacer loss coefficients as well as the friction factor relationship were also obtained from References (3) and (4).

The geometry model presented in Fig. 13 identifies the location of the subchannels. The model was a one-eighth sector of the total bundle cross section and was justifiable based on geometric symmetry as previously verified (3) and (4). Dimensions of the model were as-built dimensions measured during and after bundle assembly. The rod diameters were measured to be 1 cm (0.392 in.). The rod pitch was 1.37 cm (0.539 in.) and the rod-to-wall spacing was 0.56 cm (0.220 in.). The sleeve blockages were modeled as flow area reductions. The area reductions in the tapered region of the blockage sleeves were assumed to vary linearly along the length of the tapers.

Before comparing the measured axial velocity profiles with COBRA predictions, the local measured velocity data were used to calculate subchannel average velocities. Subchannel average velocities

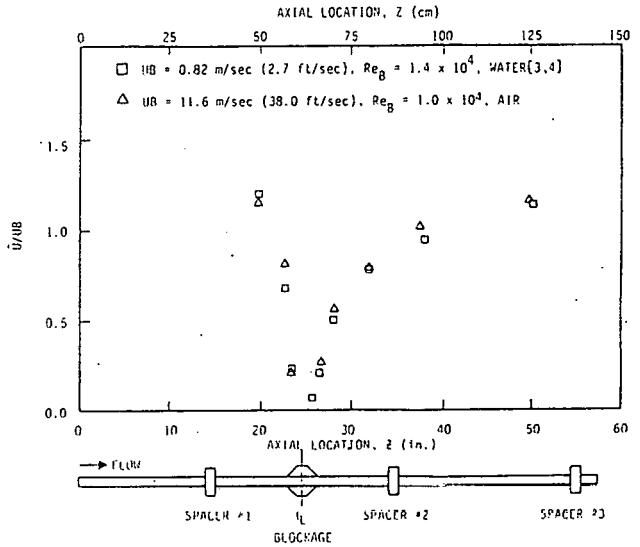

Fig. 11 Axial profiles of Subchannel 1 center velocities in air and water

were required because the COBRA code computes average values only. For Subchannels 1, 2, and 3, an area-weighting approach in conjunction with the assumption of highly turbulent flow was used to estimate subchannel average velocities from experimental local velocity data as described in detail by Creer et al. (7). Average velocities for Subchannels 4 through 10 were determined by inspecting the velocity profiles at nondisturbed data planes, e.g., DP 12, and estimating the ratio of the average subchannel velocity to the subchannel centroid velocity. Average subchannel velocities at undisturbed data planes were known to be approximately equal to the average bundle velocity. This approach was also used for Subchannels 1, 2, and 3 at locations not influenced by the blockage cluster.

COBRA Predictions

COBRA predictions of the measured air velocity data are presented in Figs. 14 and 15. In each, the ratio of average subchannel velocity to bundle average velocity is presented as a function of axial distance along the length of the bundle. The measured data points are actually subchannel average

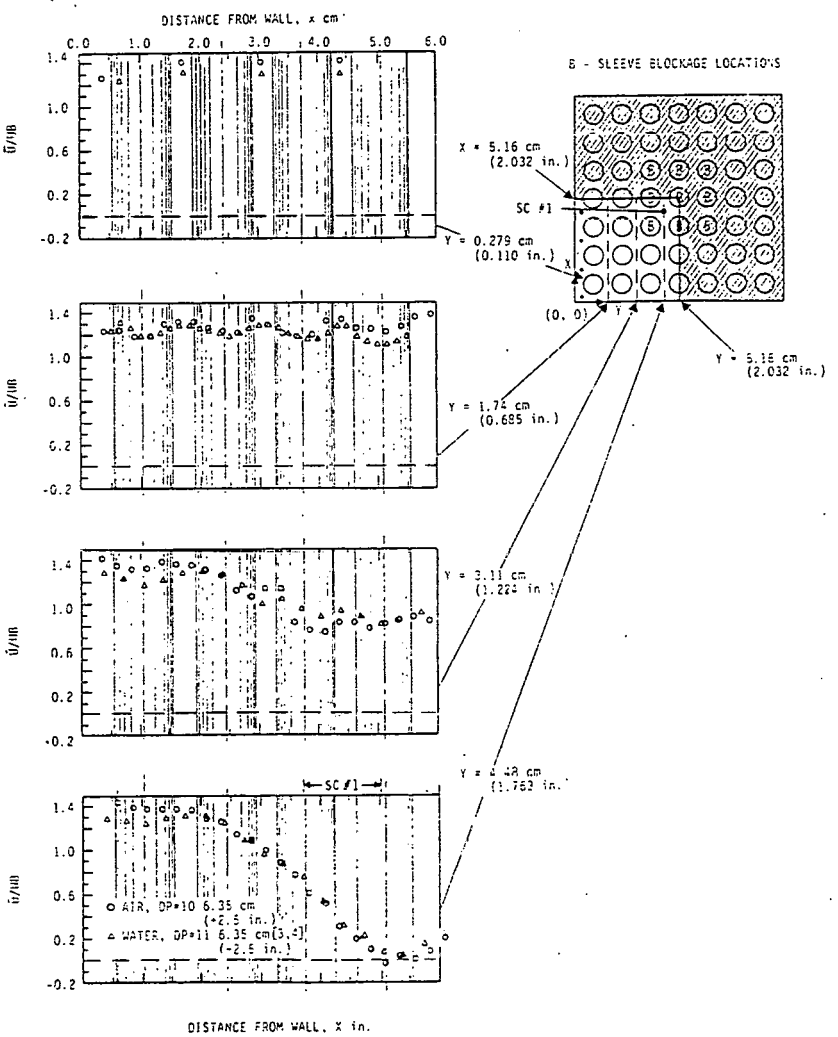

Fig. 12 Comparisons of air and water velocity profiles at a selected axial location

Table 1. COBRA Input Parameters

Parameter	COBRA Symbol	Value
Cross flow resistance	K_{ij}	0.02
Transverse momentum	s/ℓ	0.25
Turbulent momentum factor	ft	1.0
Bare rod friction factor	f	0.34 $Re^{-0.25}$
Subchannel spacer loss coefficient	K_{s1}	1.14
Subchannel blockage loss coefficient	K_{s2}	
For Subchannel 1		0.5
For Subchannel 2		0.05
Other subchannels		0.0
Model length		1.02 m (40.0 in.)
Calculation increment	Δz	1.27 cm (0.5 in.)
Total transient time	t	2.0 sec
Turbulent mixing	β	0.02
Temperature	T	27°C (80.0°F)

velocities estimated using measured local axial velocities as discussed in the previous section.

Predictions of Subchannel 1, 2, and 3 average velocities are shown in Fig. 14. COBRA predicted Subchannel 1 average velocities extremely well. The predicted normalized minimum velocity magnitude upstream of the blockage cluster was higher, 0.45 versus 0.32, than the measured value; however, the predicted minimum velocity location coincided with the measured location. Jetting predicted at the entrance to the blockage cluster was not detected experimentally. Jetting may not have been measured because the LDA measuring volume could not be positioned close enough to the blockage axial centerline. This geometrical restriction was encountered because the exterior sleeve blockages "blocked out" the incident laser beams due to the angle θ between beams.

The predicted recovery profile in Subchannel 1 downstream of the blockage was in excellent agreement with the measured profile. Again, jetting predicted at the exit of the blockage was not experimentally measured for the possible reason cited above. COBRA predictions of Subchannel 2 and 3 velocities agree satisfactorily with measured values (±10%).

Figure 15 presents COBRA predictions of average velocities in Subchannels 4, 5, and 6. The predicted velocity profiles agree well with the measured profiles. Note that estimates of measured subchannel average velocity values are slightly higher than predicted values. This trend would indicate that the predictions are low or the estimates of subchannel average velocities are high. Comparisons of COBRA predictions and experimental data obtained in Subchannels 7, 8, 9, and 10, not presented herein, were essentially the same as those for Subchannels 4, 5, and 6. In any event, COBRA can be used to satisfactorily predict average subchannel velocity values near the blockage cluster.

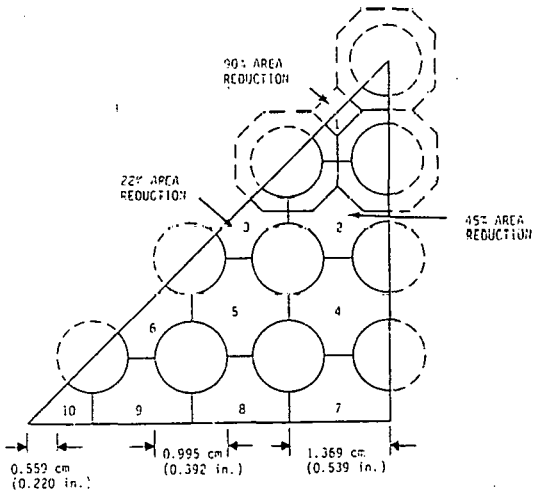

Fig. 13 COBRA geometry model at the blockage axial centerline

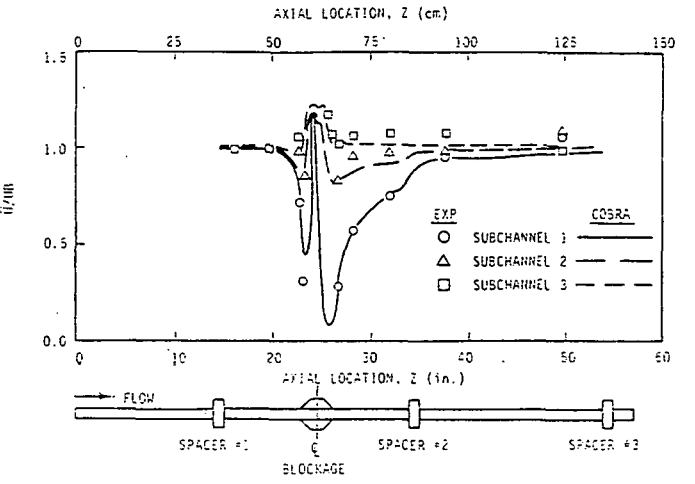

Fig. 14 COBRA velocity predictions in blocked Subchannels 1, 2, and 3 with a 90% blockage, U_B = 11.6 cm/sec (38 ft/sec)

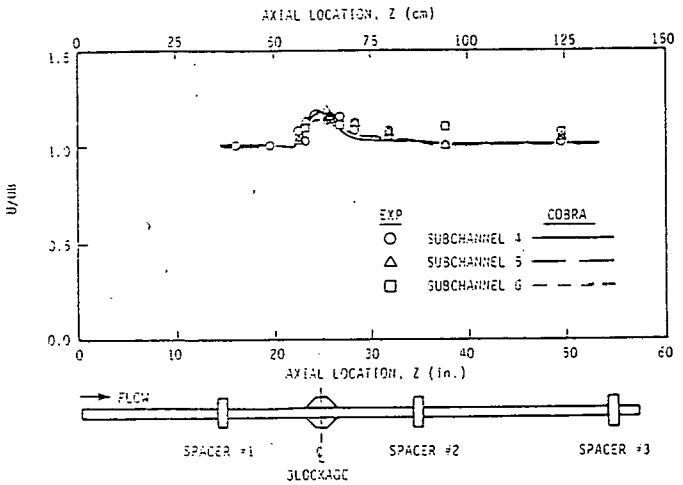

Fig. 15 COBRA velocity predictions in unblocked Subchannels 4, 5, and 6 with a 90% blockage, U_B = 11.6 m/sec (38 ft/sec)

SUMMARY AND CONCLUSIONS

This experimental study provides information regarding turbulent air flow near postulated sleeve blockages in an unheated 7x7 rod model nuclear fuel bundle. Local mean axial velocity measurements were obtained with a laser Doppler anemometer at selected axial locations in the bundle.

The experimental results indicated that a 90% blockage located midway between two grid spacers created a severe flow disturbance. Axial velocities measured immediately upstream of the blockage cluster were extremely low and flow reversals were detected downstream of the blockage. The recirculation zone existed for approximately five subchannel hydraulic diameters downstream of the blockage axial centerline. Flow recovery was completed approximately 50 subchannel hydraulic diameters downstream of the blockage. The gross influence of the blockage in the lateral direction was confined to those subchannels containing sleeve blockages. Flow increases were detected in the subchannels adjacent to the blockage cluster because flow was diverted around the cluster. The air velocity profiles were in excellent agreement with prior water velocity data obtained at approximately the same Reynolds number.

Subchannel average velocity predictions of the COBRA computer program were in good agreement with subchannel average velocities estimated using the measured local velocity data. Therefore, COBRA can be used to estimate the effects of blockages on single-phase flow distributions in rod bundles.

ACKNOWLEDGMENTS

Appreciation is extended to Dr. Stan Fabic and Dr. L. S. Tong of the U.S. Nuclear Regulatory Commission, Division of Reactor Safety Research, for sponsorship of the air flow blockage experiment. The authors wish to acknowledge the outstanding efforts of the following individuals who contributed to the success of the study: D. S. Rowe and A. M. Sutey for management support; A. J. Anthony for equipment design; K. D. Hinkle for fabrication, assembly, and installation of equipment; R. A. McBride for instrumentation setup; R. R. Dohaniuk for loop operation and data acquisition; C. A. McMonagle for COBRA velocity predictions; P. M. Crawford for manuscript typing; A. J. Currie for editing; and R. A. Keefe and S. M. Flink for word processing.

REFERENCES

1 Rowe, D. S., "COBRA-IIIC: A Digital Computer Program for Steady-State and Transient Thermal-Hydraulic Analysis of Rod Bundle Nuclear Fuel Elements," BNWL-1695, March 1973, Pacific Northwest Laboratory, Richland, Wash.

2 Wheeler, C. L., Stewart, C. W., Cena, R. J., Rowe, D. S., and Sutey, A. M., "COBRA-IV-I: An Interim Version of COBRA for Thermal-Hydraulic Analysis of Rod Bundle Nuclear Fuel Elements and Cores,"BNWL-1962, March 1976, Pacific Northwest Laboratory, Richland, Wash.

3 Creer, J. M., Rowe, D. S., Bates, J. M., and Sutey,. A. M., "Effects of Sleeve Blockages on Axial Velocity and Intensity of Turbulence in an Unheated 7x7 Rod Bundle," BNWL-1965, December 1975, Pacific Northwest Laboratory, Richland, Wash.

4 Creer, J. M., Bates, J. M., Sutey, A. M., and Rowe, D. S., "Turbulent Flow in a Model Nuclear Fuel Rod Bundle Containing Partial Flow Blockages," Nuclear Engineering and Design, Vol. 52, 1979, pp. 15-33.

5 Hardy, D. G., "High Temperature Expansion and Rupture Behavior of Zircaloy Tubing," Proceedings of Topical Meeting on Water Reactor Safety, CONF-730-304, March 1973, Salt Lake City, Utah.

6 Brayton, D. B., and Goethert, W. H., "A New Dual-Scatter Laser Doppler-Shift Velocity Measuring Technique," ISA Transactions, Vol. 10, 1971, pp. 40-50.

7 Creer, J. M., and Bates, J. M., "Effects of Sleeve Blockages on Air Velocity Distributions in an Unheated 7x7 Rod Bundle," BNWL-1975, January 1976, Pacific Northwest Laboratory, Richland, Wash.

8 Schenk, H., Jr., Theories of Engineering Experimentation, McGraw-Hill Book Company, New York, 1961, p. 40.

9 Rowe, D. S., "Measurement of Turbulent Velocity, Intensity, and Scale in Rod Bundle Flow Channels," BNWL-1736, May 1973, Pacific Northwest Laboratory, Richland, Wash.

10 Rowe, D. S., and Chapman, C. C., "Measurement of Turbulent Velocity, Intensity, and Scale in Rod Bundle Flow Channels Containing a Grid Spacer," BNWL-1757, June 1973, Pacific Northwest Laboratory, Richland, Wash.

11 Kjellstrom, B., "Studies of Turbulent Flow Parallel to a Rod Bundle of Triangular Array," STU-68-263/U210, 1971, A. B. Atomenergi, Studsvik, 611 01, Nykoping, Sweden.